Journal of Photochemistry and Photobiology A: Chemistry 217 (2011) 259–266

Contents lists available at ScienceDirect

Journal of Photochemistry and Photobiology A: Chemistry

journal homepage: www.elsevier.com/locate/jphotochem

Influence of particle size on the photoactivity of Ti/TiO_2 thin film electrodes, and enhanced photoelectrocatalytic degradation of indigo carmine dye

T.T. Guaraldo, S.H. Pulcinelli, M.V.B. Zanoni*

UNESP – Instituto de Química – Universidade Estadual Paulista Júlio de Mesquita Filho, Rua Professor Francisco Degni, s/n, 14800-900 Araraquara, SP, Brazil

ARTICLE INFO

Article history:
Received 1 June 2010
Received in revised form 16 October 2010
Accepted 21 October 2010
Available online 28 October 2010

Keywords:
Indigo carmine
Photoelectrocatalytic treatment
Nanoporous TiO_2
Nanoparticulated TiO_2
Thin films
Sol–gel

ABSTRACT

Photoanodes based on Ti/TiO_2 thin films were prepared by the sol–gel method, using either tetraisopropoxide ($Ti(OPri)_4$) or modified tetraisopropoxide, producing electrodes with different sized nanoparticle coatings, termed nanoporous (20 nm) or nanoparticulated (10 nm) electrodes. The anatase form dominated the composition of the nanoparticulated electrode, which presented a higher surface area, a flat band potential shift of −160 mV and a 50% improvement in photoactivity, compared to the nanoporous electrode. 100% color removal, and 75% mineralization, of indigo carmine dye were achieved after 15 min of photoelectrocatalytic treatment using a nanoparticulated Ti/TiO_2 electrode operated at a current density of 0.4 mA cm^{-2}. Our findings indicate that the use of nanoparticulated electrodes, under UV irradiation and with controlled current density, is an efficient alternative for the removal of food dye contaminants during wastewater treatment.

1. Introduction

The method of preparation of a semiconductor directly influences its performance in the photocatalytic oxidation of organic compounds. Among the known methods, the sol–gel procedure has been extensively used because it presents many advantages over other techniques, including sample purity, homogeneity, flexibility for introduction of dopants, even at high concentrations, control of stoichiometry and composition, ease of processing and ability to coat large and complex areas [1].

Titanium dioxide (TiO_2) has received considerable attention as a photocatalyst material, due to its good performance in treatment of organic environmental pollutants [2,3]. In a photocatalytic system, the photo-induced molecular transformation or reaction takes place at the surface of the catalyst, giving rise to the generation of electron–hole pairs under UV light irradiation. A very successful strategy to improve the efficiency of a photocatalytic system has been the application of a positive current density, which generates an electric field within the semiconductor [3,4]. Separation of the charge carriers is enhanced by the potential gradient generated as holes are driven to the catalyst surface, while electrons are efficiently driven toward the interior of the semiconductor, where they can be swept to the counter electrode through an external circuit. This arrangement improves the photocatalytic activity of TiO_2, since electron/hole pair separation is more effective, and recombination is minimized. Photoelectrocatalytic oxidation has been investigated as an attractive means of increasing the photocatalytic efficiency of organic pollutants degradation [5,6]. However, TiO_2 film physical properties, such as particle size [7,8], crystal structure [9–14], phase composition [8–14] and surface area [15,16] play an important role in the photocatalytic activity. Hence, preparation methods that consider particle size [17,18] deserve special attention. Surface properties are of paramount importance for nanosized grain materials, because the higher the surface to volume ratio, the higher the active area. It is known that control of particle morphology and surface chemistry can reduce electron–hole recombination, and also optimize surface adsorption, which could be crucial for success of the photoelectrocatalytic process.

Another parameter to be controlled is the TiO_2 catalyst composition. TiO_2 is found in three allotropic forms, anatase (tetragonal), brookite (orthorhombic) and rutile (tetragonal). The anatase form usually presents higher photoactivity than the other forms, probably because it is the most photoactive phase and has more hydroxyl groups preserved as active sites on its surface [1]. As photoactivity depends on TiO_2 crystallinity, nanostructured materials presenting small crystallite size, large surface area and high porosity are suitable for these applications. Therefore, control of both particle size and the phase composition of titanium dioxide nanoparticles, which influence electrode characteristics, is crucial in order to improve photoelectrocatalytic performance.

In this work, TiO_2 nanoparticles were prepared by the sol–gel technique, using two different methodologies: one using tetraiso-

* Corresponding author.
E-mail address: boldrinv@iq.unesp.br (M.V.B. Zanoni).

1010-6030/$ – see front matter © 2010 Elsevier B.V. All rights reserved.
doi:10.1016/j.jphotochem.2010.10.019

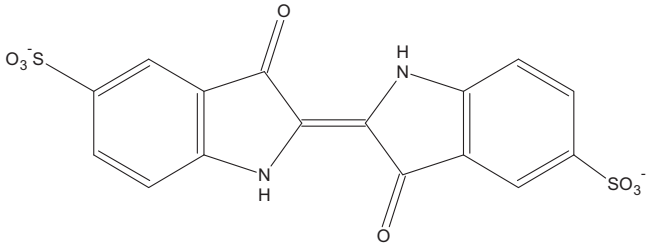

Fig. 1. Molecular formula of indigo carmine (IC) food dye.

propoxide [Ti(OProp)$_4$] as precursor [5,17], and the other using tetraisopropoxide modified by the addition of paratoluenosulfonic acid (PTSH) and acetylacetone (acac) [18]. The effects of particle size and phase composition were studied for each coated photoelectrode (Ti/TiO_2), together with photocatalytic activities. The influences of the electrodes on the photoelectrocatalytic oxidation of organic pollutants were compared, using a common food dye, indigo carmine (CI 73015) (Fig. 1) as a frequently studied model [19–24]. Most studies have only evaluated the discoloration of indigo carmine dye using TiO_2 powder catalyst [19–21], hydrogen peroxide [22,23] or the Fenton process [24]. Results for color removal have been satisfactory; however there has been no indication of any significant degree of mineralization. Considering the toxicity and carcinogenic properties of indigo carmine [25–31], the provision of efficient methods for its removal remains a challenge.

2. Experimental

2.1. Preparation of nanoporous TiO_2

The suspensions were prepared by the sol–gel process [32,33], using 0.02 L of titanium tetraisopropoxide (Aldrich), added to a solution of nitric acid in deionized water (Milli-Q) to achieve a resultant Ti:H^+:H_2O molar ratio of 1:0.5:200 (v/v/v). The precipitate obtained was continuously stirred until complete peptization produced a stable suspension, which was dialyzed in deionized water up to pH 3.5, using a Micropore (3500 MW) dialysis membrane.

2.2. Preparation of nanoparticulated TiO_2

Titanium tetraisopropoxide (Ti(OPri)$_4$) solution was slowly added to a mixture of acetylacetone/isopropanol (molar ratio = 1), at room temperature with stirring. The clear mixture was subsequently added dropwise to an aqueous solution of paratoluene–sulfonic acid (PTSH). The acidified (pH 2.3) solution was refluxed for 18 h at 60 °C, under magnetic stirring. The flask was fitted with a $CaCl_2$ trap to avoid exposure to moisture. The molar ratios used were PTSH/Ti = 0.2 and H_2O/Ti = 4 (v/v) [18].

2.3. Preparation of nanoporous and nanoparticulated Ti/TiO_2 thin-film electrodes

Photoelectrodes of nanoporous and nanoparticulated Ti/TiO_2 were prepared according to the procedure previously described in the literature [32,33]. The thin-film photoelectrodes were formed by dip coating at a constant velocity (100 mm min^{-1}) onto a titanium foil (25.0 cm^2 and 0.5 mm thickness, Goodfellow Cambridge Ltd.). A sequence of dipping, drying (at 100 °C for 1 h) and firing (at 450 °C for 3 h) was used for each coating (five repetitions), according to the procedure described earlier [32,33].

2.4. Apparatus and procedure

The photoelectrocatalytic oxidation experiments were performed in a 1-L capacity PVC (polyvinylchloride) reactor, operating as a single compartment cell. A Ti/TiO_2 photoanode, acting as working electrode of TiO_2 (25 cm^2), and an auxiliary electrode of Pt gauze, were arranged around the lamp (80 W, Philips medium pressure mercury, I = 2.732 mW cm^{-2}), which was inserted into a quartz tube, separated from the photoanode by a distance of 2.5 cm. This system produced irradiation in the range 315–200 nm. All the measurements were carried out after filling the reactor with a solution of 5.35×10^{-5} mol L^{-1} dye in 0.1 mol L^{-1} aqueous sodium sulfate (Na_2SO_4). The photoelectrocatalytic measurements were conducted while bubbling compressed air through a small tube.

A galvanostat (AUTOLAB Model PGSTAT 302), controlled by GPES software, was used to bias the photoanode during the photoelectrocatalytic oxidation experiments. All the pH measurements were carried out using a Corning 555 pH meter.

The indigo carmine dye concentrations were monitored in a quartz cell, using a Hewlett Packard 8453 spectrophotometer operating between 190 and 800 nm. Measurements of total organic carbon were used to monitor the degree of mineralization (Shimadzu TOC-V_{CPN} analyzer). A high performance liquid chromatograph (Shimadzu Model 10AVP), equipped with a photodiode array detector, was used to separate and identify the IC dye during the oxidation process. The separation column was a G-ODS (4 mm × 250 mm, 5 nm), and the mobile phase was phosphate (3.0×10^{-4} mol L^{-1})/methanol, at a ratio of 70:30, flowing at 0.5 mL min^{-1} at room temperature.

The photoelectrodes were characterized by X-ray powder diffraction (XRPD), using a Siemens D5000 diffractometer (λ = 1.541 Å) with (CuKα) graphite monochromatized radiation. The surface morphology was investigated by both scanning electron microscopy (JEOL JSM-T330A) and atomic force microscopy (Digital Instruments – Veeco MultiMode Nanoscope IIIa), operating in contact (Veeco NP N_3Si_4 probe) and tapping (Nanoworld NCH silicon probe) modes.

3. Results and discussion

3.1. Photoanode characteristics

The surface porosity characteristics of both Ti/TiO_2 electrodes, prepared by the sol–gel method using either tetraisopropoxide or modified tetraisopropoxide as precursor (denoted nanoporous and nanoparticulated electrodes, respectively), were analyzed by scanning electron microscopy and are compared in Fig. 2. The electrodes exhibited high homogeneity but different morphologies. Small clusters of titanium crystals were easily observed on the nanoparticulated electrode (curves C and D), while the nanoporous film (curves A and B) showed a cracked mud appearance with no visible particles on its surface. This was confirmed by the 3D topography of the TiO_2 thin films obtained from AFM measurements (Fig. 3). Except for the metallic titanium sample, whose surface was not coated with any TiO_2 thin film, the surfaces of the electrodes treated at 450 °C showed particular nanostructural features, such as a high density of grains with nanometric dimensions. The grain analysis (Fig. 3) of nanoporous (A), nanoparticulated (B) and metallic Ti (C) materials, performed at the 2.0 μm × 2.0 μm scale using the tapping mode, indicated that both nanostructured films possessed homogeneous geometry and a compact arrangement. Thicknesses of around 10 μm and 15 μm were estimated for the nanoporous and nanoparticulated electrodes, respectively. The amount of TiO_2 anchored on the Ti foil surface area was estimated to be around 152 g m^{-2} and 164 g m^{-2} for nanoporous and nanoparticulated photoanodes, respectively.

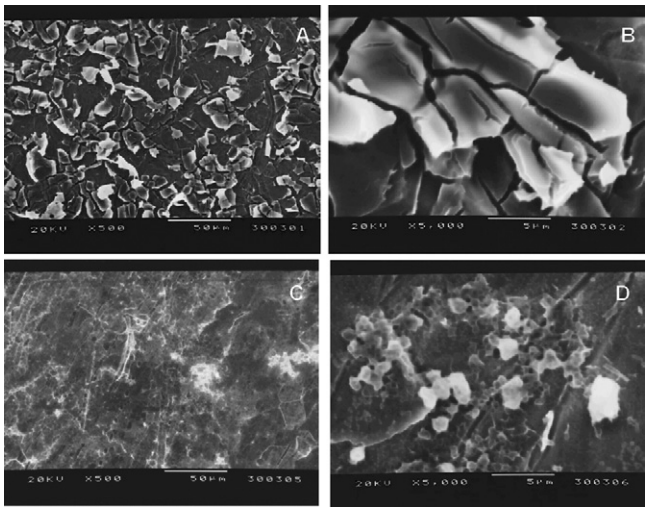

Fig. 2. Scanning electron microscopy (SEM) images of the nanoporous (A and B) and nanoparticulated (C and D) materials, at different magnifications (500× and 5000×).

Fig. 4 shows the X-ray diffraction patterns of both TiO_2 thin films supported on titanium, with the presence of characteristic peaks of the two expected phases, rutile ($2\theta = 28$) and anatase ($2\theta = 25$). All the peak characteristics of the metallic titanium phase are indicated as Ti (ASTMPDF). The peaks observed at $2\theta = 25$ and $2\theta = 28$ can be attributed to the anatase (A) and rutile (R) phases, respectively, taking account of the well known convolution of peaks assigned by the mixed symbol. This indicates that both electrodes were formed of a mixture of allotropic titanium phases. Considering the relative intensities of these peaks, the proportion of each phase could be calculated by integrating their areas. Results showed that for the nanoporous electrode (X), the anatase/rutile phase proportion was equal to 0.25, while for the nanoparticulated (Y) electrode the proportion increased to almost 1.7.

The average crystallite size, representing the size of the domain possessing crystalline structure, was also calculated for both A and R peaks of each electrode. Assuming that the width of these peaks was determined only by a size effect, the crystallite size was calculated using the Scherrer formula [34], in which this size is inversely proportional to the width at half height. The values obtained were 20 and 10 nm, for the nanoporous and nanoparticulated electrodes, respectively.

3.2. Photoactivity of nanoporous and nanoparticulated electrodes

Fig. 5 illustrates the linear voltammograms obtained for the nanoporous and nanoparticulated Ti/TiO_2 electrodes in 0.1 mol L^{-1} Na_2SO_4, at pH 2.0, with and without UV irradiation. Under UV irradiation, both electrodes presented a typical photocurrent expected for n-type semiconductor photoanodes [3,4]. Although the electrodes had similar geometric areas, the photocurrent was almost two times higher for the nanoparticulated electrode. This suggests higher e^-/h^+ charge separation, and lower recombination rates, on nanoparticulated electrodes, as expected because the surface area of the film increases for smaller particle sizes and higher porosities.

Although the photocurrent onset potential (E_{on}) is often designated as the flat band potential (E_{fb}), there are large uncertainties in these measurements, since recombination can suppress the photocurrent in the vicinity of E_{fb} [3]. Butler [36] has described an extrapolation procedure to determine E_{fb}, based on curves of photocurrent *vs.* potential using the following equation: ; where I_{ph} = photocurrent density, q = electron charge, ε = dielectric constant, ε_0 = permittivity of free space, I_0 = photon flux, α = absorption coefficient for solids, N_d = effective density of states at the conduction band edge, E = potential, E_{fb} = flat band potential. Fig. 6 shows a plot of the square of the photocurrent *vs.* potential, which produces a straight line with intercept E_{fb}. From these graphs, flat band potential values of around −98 mV and −170 mV *vs.* Ag/AgCl were obtained for nanoporous and nanoparticulated electrodes, respectively. These values are in agreement with the different flat band potentials reported in the literature for anatase and rutile [35].

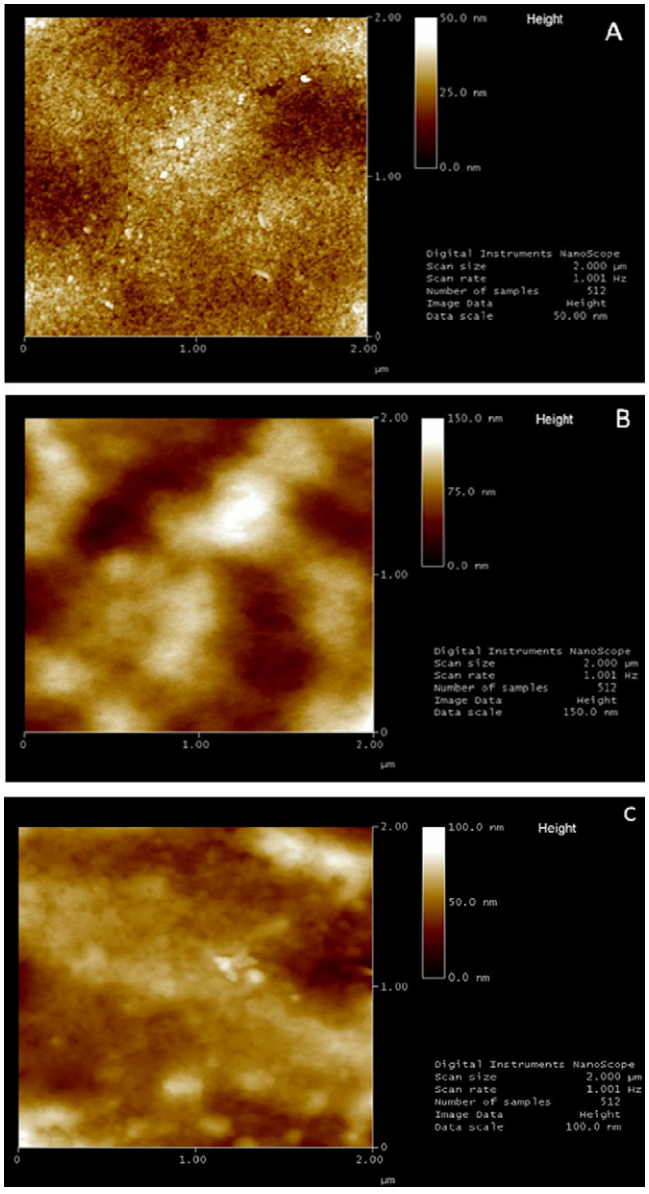

Fig. 3. Atomic force microscopy (AFM) images of the Ti metallic substrate (A), and the nanoporous (B) and nanoparticulated (C) electrodes. Scan area 30.0 µm × 30.0 µm.

The possible effect of IC dye adsorption on the Ti/TiO_2 thin-film electrodes was investigated using photocurrent *vs.* potential curves recorded either in the absence of dye, or with different dye concentrations, using linear sweep voltammetry (LSV) in 0.1 mol L^{-1} Na_2SO_4 electrolyte, at a scan rate of 10 mV s^{-1}. The photocurrent decreased markedly when the concentration of IC in solution increased (Fig. 7), indicating strong dye adsorption onto the TiO_2 surface or transparency loss due to dye coloration. Adsorption is critical for the photoelectrocatalytic oxidation process. The Langmuir–Hinshelwood (L–H) model [37] was used to

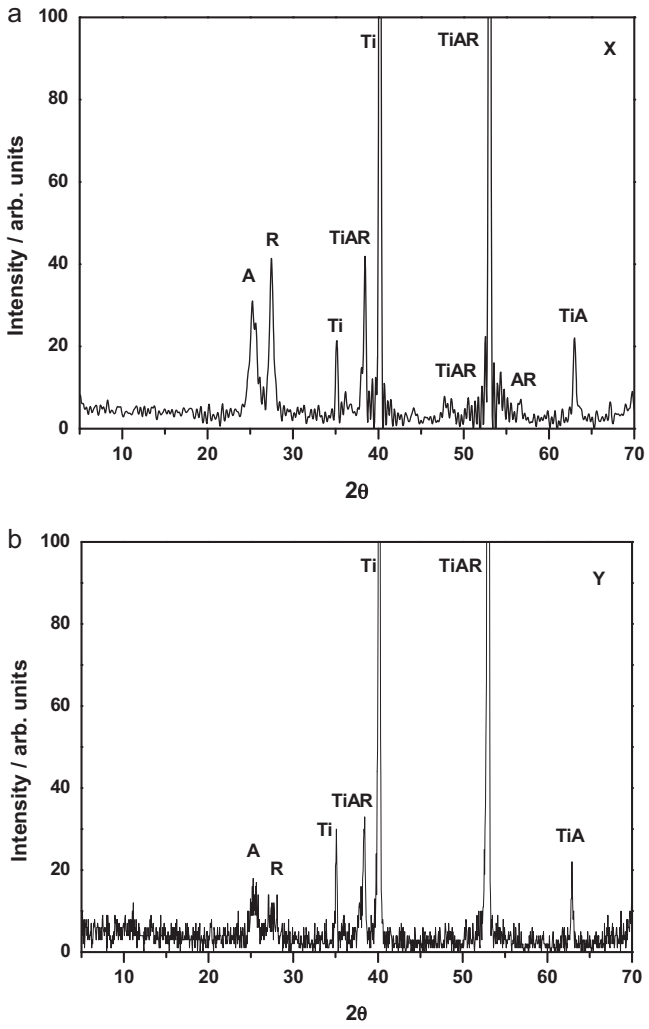

Fig. 4. X-ray diffraction of semiconductors fired at 450 °C for 3 h, prepared by the sol–gel method as nanoporous (a) and nanoparticulated (b) materials.

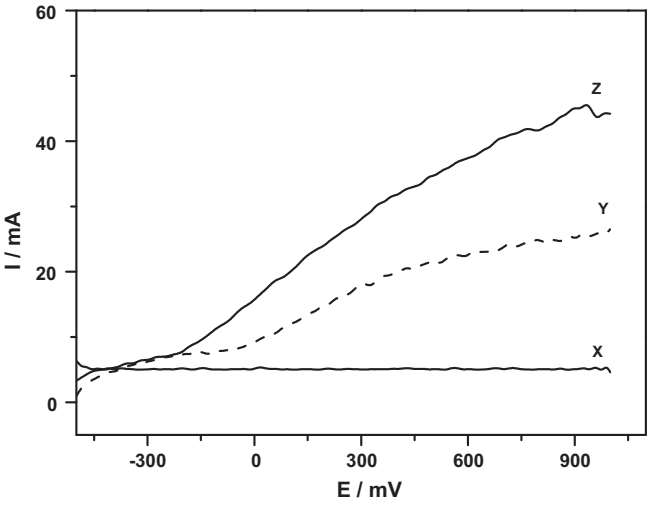

Fig. 5. Linear scan voltammograms obtained for TiO_2 thin film electrodes, in 0.1 mol L^{-1} Na_2SO_4, without irradiation (a) and under UV irradiation for the nanoporous (b) and the nanoparticulated (c) electrodes. Scan rate = 10 mV s^{-1}.

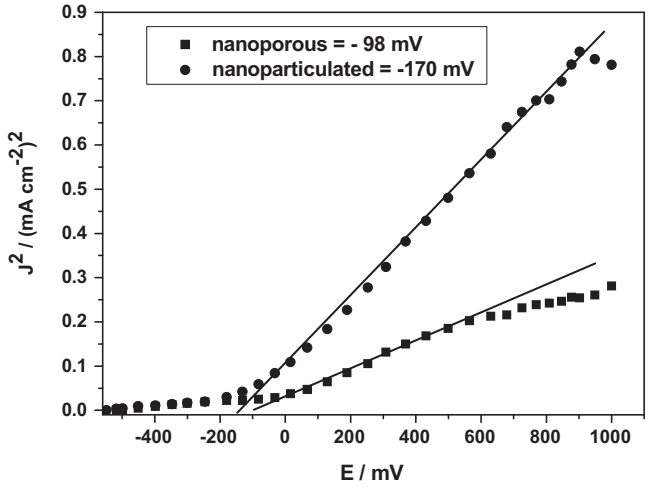

Fig. 6. The square wave of the photocurrent *vs.* applied potential for nanoporous (a) and nanoparticulated (b) TiO_2 electrodes in Na_2SO_4 under UV irradiation.

describe the dye photooxidation kinetics on both electrodes. In the L–H model, $1/I_{ph} = 1/k + [(1/kKC)]$, where k = oxidation rate constant, K = adsorption constant and C = concentration (mol L^{-1}). The plot of $1/Ip_{hs}$ *vs.* $1/C$ for IC dye was linear up to 1×10^{-4} mol L^{-1}, with regression coefficients greater than 0.988. The adsorption constants (insert of Fig. 7) estimated from the L–H model were 0.0208 mM^{-1} and 0.0724 mM^{-1}, for nanoporous and nanoparticulated electrodes, respectively, indicating that the adsorption of IC was favored on the surface of small particles.

3.3. Influence of the photoanode on the degradation of indigo carmine dye

The UV–Vis spectra obtained before, and 90 min after, photoelectrocatalytic oxidation of IC (5.35×10^{-5} mol L^{-1}) in Na_2SO_4 (0.1 mol L^{-1}) on the nanoparticulated anode are shown in Fig. 8A. The initial constant rate for this electrode is 5.0×10^{-2} min^{-1} which is referred to the decolorization process during the first

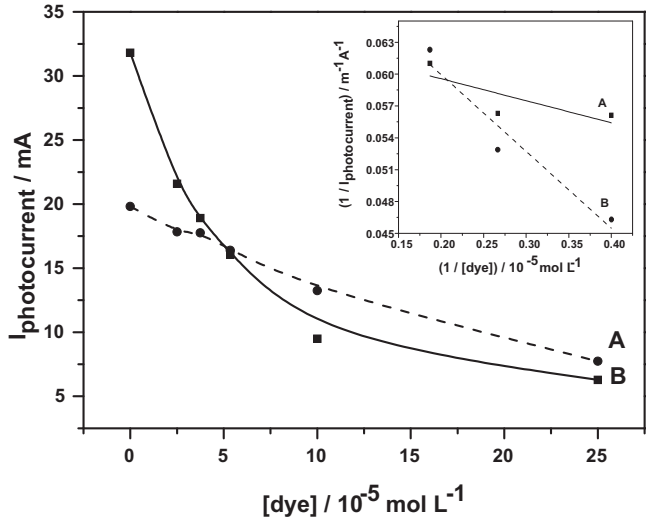

Fig. 7. Influence of indigo carmine dye concentration, from 0 to 2.50×10^{-4} mol L^{-1}, on the photocurrent measured at +1.0 V for nanoporous (A) and nanoparticulated (B) electrodes in 0.1 mol L^{-1} Na_2SO_4, pH 2.0, under UV irradiation. Scan rate = 10 mV s^{-1}. The insert shows the adsorption kinetics for the nanoporous electrode (A) and the nanoparticulated electrode (B), calculated using the Langmuir–Hinshelwood (L–H) model, according to the equation $1/Iph = 1/k + (1/kKC)$.

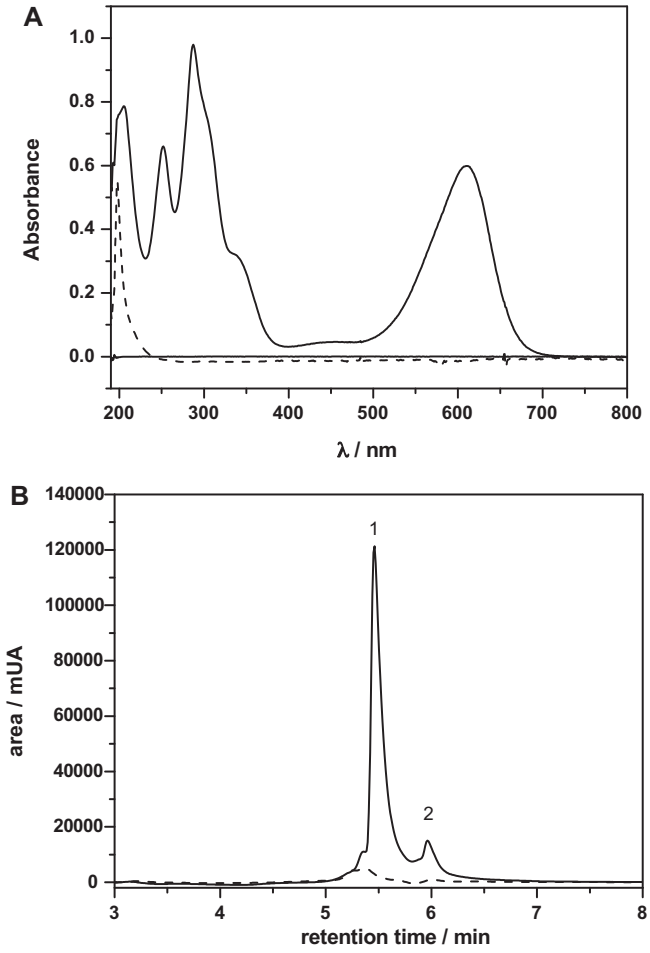

Fig. 8. UV–Vis spectra (A) and liquid chromatograms with diode array detector (B), recorded for 5.35×10^{-5} mol L^{-1} indigo dye in 0.1 mol L^{-1} Na_2SO_4, before (1) and after (2) 90 min of photoelectrocatalytic treatment of nanoparticulated electrodes, using a constant current density of 0.4 mA cm^{-2} and with UV irradiation.

15 min of oxidation. There was total suppression of the maximum absorption band at 610 nm, attributed to the chromophore site, and of the bands at 340 and 286 nm, associated with other aromatic centers in the molecule. The degradation rate of the total oxidation process is 33.0×10^{-2} min^{-1} after 90 min of treatment. Fig. 8B displays HPLC (diode array detector) chromatograms of the photoelectrocatalytic products, obtained before and after treatment. The original sulfate solution exhibits an intense peak at the IC dye retention time [t_r = 5.45 min (A = 120,000)], detectable up to 5.0×10^{-7} mol L^{-1}. This peak intensity was drastically reduced during photoelectrocatalytic treatment. Similar results were obtained for the nanoporous electrode. Peak 2 can be attributed to the contaminant of the dye [t_r = 5.97 min].

Fig. 9(curves A and B) shows fractional conversion plots relating the IC dye concentration ($\eta = ([C] - [C]_0)/[C]$) with concentrations at time t [C] and at time zero [C]$_0$, during spectrophotometric measurements taken at 610 nm for both electrodes, where it is possible to get 100% of discoloration after 30 min of treatment. The discoloration follows a first order kinetic and the rate constant was 2.4×10^{-2} min^{-1} and 3.0×10^{-2} min^{-1}, respectively for nanoparticulated and nanoporous electrodes. The dye removal was also monitored by HPLC-DAD and it was possible to reach 100% and 90%, after 300 min of treatment, respectively. Total organic carbon (TOC) concentrations, for the same solutions, are also presented in Fig. 9(curves C and D). TOC removal was around 20% higher for the nanoparticulated anode, indicating that smaller size TiO_2 coatings

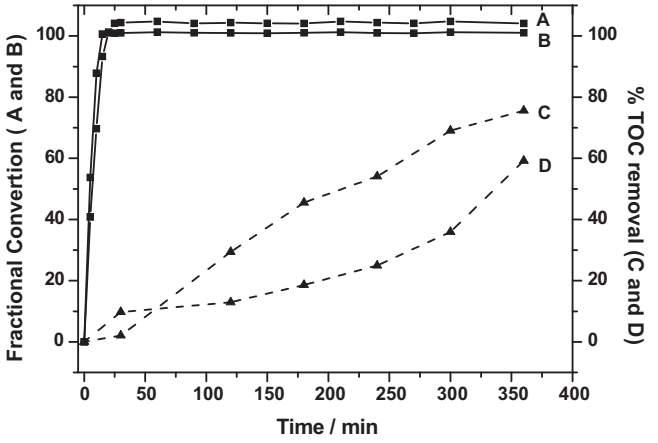

Fig. 9. Degradation of 5.35×10^{-5} mol L^{-1} of indigo carmine dye, monitored by absorption band at 610 nm, on nanoporous (A) and nanoparticulated (B) electrodes, and percentage of TOC removal on nanoporous (C) and nanoparticulated (D) electrodes.

are more effective for organic pollutant mineralization. The mineralization follows a first order process observed, which rate constant is 1.5×10^{-3} min^{-1} and 2.2×10^{-3} min^{-1} for nanoparticulated and nanoporous electrodes, respectively.

3.4. Effect of pH

The influence of pH (in the range 2–10) on the discoloration rate of IC dye (5.35×10^{-5} mol L^{-1}) in Na_2SO_4 (0.1 mol L^{-1}) was investigated for both the nanoporous and nanoparticulated electrodes. Discoloration at all pH values was only observed for the nanoparticulated electrode. The time dependence of the initial degradation rate, evaluated from the slopes of the curves obtained for dye consumption (mol L^{-1}) at each pH, was calculated for the different electrodes. The results obtained (Table 1) were in agreement with a pseudo first order reaction. The initial degradation rate was much higher at pH 2.0 for both electrodes, however the rate constant was about 37% greater for the nanoparticulated electrode, compared to the nanoporous system. This suggests that, in an acidic medium, the anionic form of the dye (pK_a = 1.2) is more strongly adsorbed on the electrode surface (zeta potential = 5.0), when positively charged, in good agreement with previous results [5,17]. Hence, pH 2.0 was chosen as the optimum for photoelectrocatalysis of the IC dye. An advantage was that there was no need for pH correction during the treatment.

3.5. Effect of controlled current density

Most photoelectrocatalytic systems are based on application of an anodic bias potential higher than the flat-band potential of the Ti/TiO_2 electrode. A potential gradient within the photocatalyst film is provided under potentiostatic conditions, to efficiently force the electrons to reach the counter electrode. Photogenerated holes can therefore be trapped in the surface by H_2O/OH^- species, giving rise to OH$^\bullet$ radicals, which are essential for promoting the efficient degradation of dyes. This work investigates a photoelectrocatalytic system in the galvanostatic mode, operating with two electrodes (working and counter electrode) under controlled anodic current density.

The effect of controlled current density (0.2, 0.4, 0.5, 0.6 and 0.8 mA cm^{-2}) on the initial degradation rate of IC dye (5.35×10^{-5} mol L^{-1}) was tested for both electrodes, in Na_2SO_4 (0.1 mol L^{-1}) at pH 2.0. As discussed previously, the discoloration followed a pseudo first order kinetics, with initial degradation rates

Table 1
Effect of pH, current density (J) and initial dye concentration (C) on the degradation kinetics (min^{-1}) of indigo carmine on nanoporous (a) and nanoparticulated (b) electrodes.

pH[a]			Current density (J) ($mA\,cm^{-2}$)[b]			Dye concentration (C) ($mol\,L^{-1}$)[c]		
pH[a]	k_a	k_b	J[b]	k_a	k_b	C[c]	k_a	k_b
2.0	24×10	38×10	0.2	16×10	27×10	25×10^{-5}	70×10^{-2}	63×10^{-2}
4.0	10×10	10×10	0.4	18×10	33×10	30×10^{-5}	31×10^{-2}	40×10^{-2}
6.0	10×10	10×10	0.5	16×10	27×10	54×10^{-5}	25×10^{-2}	30×10^{-2}
8.0	10×10	10×10	0.6	29×10	24×10	10×10^{-4}	10×10^{-2}	20×10^{-2}
10.0	10×10	10×10	0.8	28×10	37×10	25×10^{-4}	3×10^{-2}	8×10^{-2}

[a] 5.35×10^{-5} mol L^{-1} of IC in 0.1 mol L^{-1} Na_2SO_4, current density of 2.0 mA cm^{-2}.
[b] 5.35×10^{-5} mol L^{-1} of IC in 0.1 mol L^{-1} Na_2SO_4, pH 2.0.
[c] 0.1 mol L^{-1} Na_2SO_4, pH 2.0, current density of 2.0 mA cm^{-2}.

(Table 1) indicating that the maximum discoloration rate occurred with the nanoparticulated electrode, at 0.8 mA cm^{-2}.

The influence of current density on the degree of TOC removal showed some important differences. For both electrodes, maximum mineralization was achieved at a current density of 0.4 mA cm^{-2}, with values 10% higher for the nanoparticulated electrode. At higher current densities, there was concomitant liberation of oxygen gas, which competes with hydroxyl radical formation on the electrode surface, hence decreasing efficiency.

The current efficiency was estimated considering the values of total organic carbon (TOC) reached after photoelectrochemical treatment, using the following equation [38]:

$$CE(\%) = \frac{\{[(TOC)_0 - (TOC)_t]\, x\, [FV \quad 100]\}}{8I\Delta t}$$

where $(TOC)_0$ and $(TOC)_t$ are the total organic carbon ($g\,L^{-1}$) at times 0 and t, respectively, I is the current (A), F is the Faraday constant (26.8 Ah), V is the volume (L) and Δt is the time of treatment (h). The results are shown in Fig. 10 (curves X and Y, for the nanoporous and nanoparticulated electrodes, respectively). For both electrodes, a current efficiency of 75–80% was reached at a controlled current density of 0.4 mA cm^{-2}, after a treatment time of around 60 min. These results indicate that it is possible to simplify the photoelectrochemical reactor, using low current density instead of applied potential, since the latter requires a reference electrode to control the applied potential.

3.6. Effect of dye concentration

The influence of initial IC dye concentration on the photoelectrocatalytic oxidation was investigated in order to optimize the efficiency of the photoelectrodes. In the concentration range from 2.5×10^{-5} mol L^{-1} to 1.0×10^{-4} mol L^{-1}, in Na_2SO_4 (0.1 mol L^{-1}) under constant current density (0.4 mA cm^{-2}), there was complete discoloration. Degradation rate values calculated for both electrodes are compared in Table 1. The results suggest that the photoelectrocatalytic process was more effective at low dye concentrations, probably due to the transparency of the solution. The dye degradation rate was 20% faster for the nanoparticulated compared to the nanoporous electrode, with fast degradation obtained at initial dye concentrations of up to 1.0×10^{-4} mol L^{-1}, although the system required a longer treatment time.

3.7. Comparison of photolysis, photocatalysis and photoelectrocatalysis treatments

In order to test the influence of the applied current density on the photoelectrocatalyst, the degradation process of the IC dye (at a concentration of 5.35×10^{-5} mol L^{-1}, in 0.1 mol L^{-1} Na_2SO_4 at pH 2.0 was compared with systems employing photocatalysis (UV + semiconductor) and photolysis (UV). TOC removals obtained during 90 min treatment using photolysis (curve A), photocatalysis (curves B and C) and photoelectrocatalysis (curves D and E) are compared in Fig. 11. For both electrodes, the degree of mineralization was higher for the photoelectrocatalysis treatment, with 73% and 60% of TOC removal using the nanoparticulated and nanoporous electrodes, respectively. Maximum values achieved using photolysis and photocatalysis were around 20–30%. The photoelectrocatalysis technique is therefore not only efficient in decolorization, but also in mineralization of the organic material.

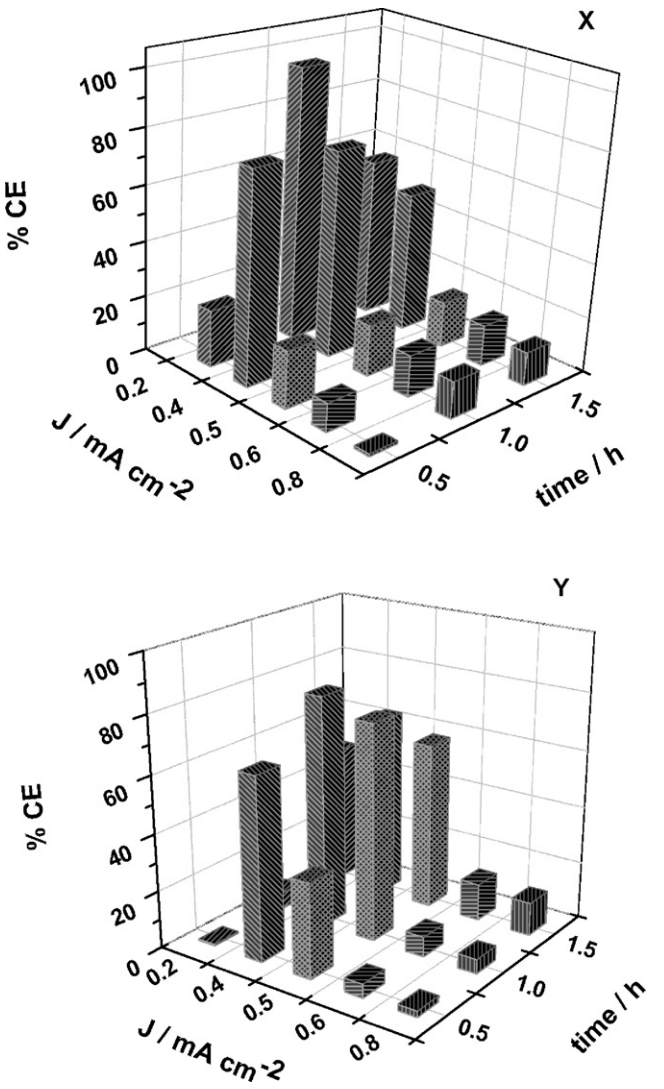

Fig. 10. Current efficiency evaluated during photoelectrocatalytic oxidation of 5.35×10^{-5} mol L^{-1} dye in 0.1 mol L^{-1} Na_2SO_4, at pH 2.0, on nanoporous (X) and nanoparticulated (Y) electrodes.

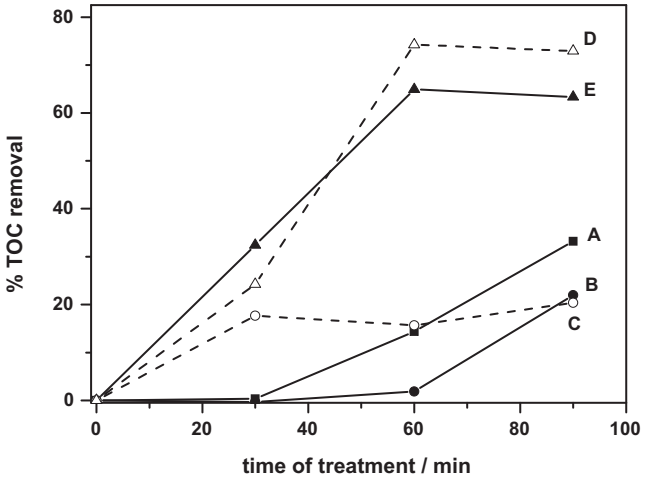

Fig. 11. TOC removal obtained during degradation of 5.35×10^{-5} mol L^{-1} dye in 0.1 mol L^{-1} Na_2SO_4, at pH 2.0, using photolysis (A), photocatalysis on nanoporous (B) and nanoparticulated (C) electrodes, and photoelectrocatalysis on nanoporous (E) and nanoparticulated (D) electrodes, under a current density of 0.4 mA cm^{-2}.

The nanoparticulated electrode showed enhanced performance during dye treatment.

4. Conclusions

Photoanodes with different particle sizes, prepared by the sol–gel method, exhibited different morphologies, but high homogeneity. Both of the electrodes studied presented good activity for dye destruction, with the electrode produced with smaller nanoparticles exhibiting a two times enhancement of photoactivity. Both Ti/TiO_2 coatings resulted in 100% color removal of indigo carmine dye, during a short period (15–20 min) of photoelectrocatalytic treatment under optimized conditions, achieving 60% and 73% mineralization for the nanoporous and nanoparticulated electrodes, respectively. This removal rate is much higher than those previously reported in the literature. The experimental conditions were optimized for maximum degradation kinetics on nanoparticulated Ti/TiO_2, acting as anode electrode, with Pt as counter electrode. The optimized conditions using UV irradiation were an IC dye concentration of 5.35×10^{-5} mol L^{-1}, pH of 2.0, and constant current density of 0.4 mA cm^{-2}. Our findings indicate that the use of controlled current density is simpler, cheaper and easier to adapt to industrial treatments, while the photoelectrodes prepared with nanoparticulated material provided greatest method efficiency. Photoelectrocatalytic oxidation could be an effective alternative for removal of food dye contaminants during wastewater treatment.

Acknowledgements

The authors thank FAPESP, CNPq and CAPES for the financial support of this work.

References

[1] O. Carp, C.L. Huisman, A. Reller, Photoinduced reactivity of titanium dioxide, Prog. Solid State Chem. 32 (2004) 33–177.
[2] K. Rajeshwar, M.E. Osugi, W. Chanmanee, C.R. Chenthamarakshan, M.V.B. Zanoni, P. Kajitvichyanukul, R. Krishnan-Ayer, Heterogeneous photocatalytic treatment of organic dyes in air and aqueous media, J. Photochem. Photobiol. C 9 (2008) 171–192.
[3] H.O. Flinkea (Ed.), Semicondutor Photoelectrochemistry, Elsevier, Amsterdam, 1988.
[4] P.A. Christensen, T.A. Egerton, S.A.M. Kosa, J.R. Tinlin, K. Scott, The photoelectrocatalytic oxidation of aqueous nitrophenol using a novel reactor, J. Appl. Electrochem. 35 (2005) 683–692.
[5] M.V.B. Zanoni, J.J. Sene, M.A. Anderson, Photoelectrocatalytic degradation of remazol brilliant orange 3R on titanium dioxide thin-film electrodes, J. Photochem. Photobiol. A 157 (2003) 55–63.
[6] M.E. Osugi, K. Rajeshwar, D.P. Oliveira, A.R. Araujo, E.R. Ferraz, M.V.B. Zanoni, Comparison of oxidation efficiency of disperse dyes by chemical and photoelectrocatalytic chlorination and removal of mutagenic activity, Electrochim. Acta 54 (2009) 2086–2093.
[7] Z.B. Zhang, C.C. Wang, R. Zakaria, J.Y. Ying, Role of particle size in nanocrystalline TiO_2-based photocatalysts, J. Phys. Chem. B 102 (1998) 10871–10878.
[8] H.D. Jang, S.-K. Kim, S.-J. Kim, Effect of particle size and phase composition of titanium dioxide nanoparticles on the photocatalytic properties, J. Nanopart. Res. 3 (2001) 141–147.
[9] R.I. Bickley, T. Gonzalez-Carreno, J.S. Lees, L. Palmisano, R.J.D. Tilley, A structural investigation of titanium dioxide photocatalysts, J. Solid State Chem. 92 (1991) 178–190.
[10] A.L. Linsebigler, G.Q. Lu, J.T. Yates, Photocatalysis on TiO_2 surfaces: principles, mechanisms, and selected results, Chem. Rev. 95 (1995) 735–758.
[11] S.S. Watson, D. Beydoun, J.A. Scott, R. Amal, The effect of preparation method on the photoactivity of crystalline titanium dioxide particles, Chem. Eng. J. 95 (2003) 213–220.
[12] S.K. Lee, P.K.J. Robertson, A. Mills, D. McStay, N. Elliott, D. McPhail, The alteration of the structural properties and photocatalytic activity of TiO_2 following exposure to non-linear irradiation sources, Appl. Catal. B 44 (2003) 173–184.
[13] A. Sclafani, J.M. Herrmann, Comparison of the photoelectronic and photocatalytic activities of various anatase and rutile forms of titania in pure liquid organic phases and in aqueous solutions, J. Phys. Chem. 100 (1996) 13655–13661.
[14] M.H. Habibi, H. Vosooghian, Photocatalytic degradation of some organic sulfides as environmental pollutants using titanium dioxide suspension, J. Photochem. Photobiol. A 174 (2005) 45–52.
[15] B. Ohtani, S. Zhang, J. Handa, H. Kajiwara, S. Nishimoto, T. Kagiya, Photocatalytic activity of titanium(IV) oxide prepared from titanium(IV) tetra-2-propoxide: reaction in aqueous silver salt solutions, J. Photochem. Photobiol. A 64 (1992) 223–230.
[16] G. Dagan, M. Tomkiewicz, TiO_2 aerogels for photocatalytic decontamination of aquatic environments, J. Phys. Chem. 97 (1993) 12651–12655.
[17] P.A. Carneiro, M.E. Osugi, J.J. Sene, M.A. Anderson, M.V.B. Zanoni, Evaluation of color removal and degradation of a reactive textile azo dye on nanoporous TiO_2 thin-film electrodes, Electrochim. Acta 49 (2004) 3807–3820.
[18] R.C. Kaminski, S.H. Pulcinelli, A.F. Craievich, C.V. Santilli, Nanocrystalline anatase thin films prepared from redispersible sol–gel powders, J. Eur. Ceram. Soc. 25 (2006) 2175–2180.
[19] M. Vautier, C. Guillard, J.-M. Herrmann, Photocatalytic degradation of dyes in water: case study of indigo and of indigo carmine, J. Catal. 201 (2001) 46–59.
[20] N. Barka, A. Assabbane, A. Nounah, Y.A. Ichou, Photocatalytic degradation of indigo carmine in aqueous solution by TiO_2-coated non-woven fibers, J. Hazard. Mater. 152 (2008) 1054–1059.
[21] L.L. Costa, A.G.S. Prado, TiO_2 nanotubes as recyclable catalyst for efficient photocatalytic degradation of indigo carmine dye, J. Photochem. Photobiol. A 201 (2009) 45–49.
[22] A.H. Gemeay, I.A. Mansour, R.G. El-Sharkawy, A.B. Zaki, Kinetics and mechanism of the heterogeneous catalyzed oxidative degradation of indigo carmine, J. Mol. Catal. A: Chem. 193 (2003) 109–120.
[23] C. Galindo, P. Jacques, A. Kalt, Photochemical and photocatalytic degradation of an indigoid dye: a case study of acid blue 74 (AB74), J. Photochem. Photobiol. A 141 (2001) 47–56.
[24] C. Flox, S. Ammar, C. Arias, E. Brillas, A.V. Vargas-Zavala, R. Abdelhedi, Electro-Fenton and photoelectro-Fenton degradation of indigo carmine in acidic aqueous medium, Appl. Catal. B 67 (2006) 93–104.
[25] D.L. Jeffords, P.H. Lance, W.C. Dewolf, Severe hypertensive reaction to indigo carmine, Urology 9 (1977) 180–181.
[26] J.C. Erickson, B.A. Widmer, The vasopressor effect of indigo carmine, Anesthesiology 29 (1968) 188–189.
[27] W.F. Kennedy, K. Wirjoatmadja, T.J. Akamatsu, J.J. Bonica, Cardiovascular and respiratory effects of indigo carmine, J. Urol. 100 (1968) 775–778.
[28] T.Y. Ng, T.D. Datta, B.I. Kirimli, Reaction to indigo carmine, J. Urol. 116 (1976) 132–133.
[29] K. Ikeda, Y. Sannohe, S. Araki, S. Inutsuka, Intra-arterial dye method with vasomotors (PIAD method) applied for the endoscopic diagnosis of gastric cancer and the side effects of indigo carmine, Endoscopy 14 (1982) 119–123.
[30] J. Hooson, I.F. Gaunt, I.S. Kiss, P. Grasso, K.R. Butterworth, Long-term toxicity of indigo carmine in mice, Food Cosmet. Toxicol. 13 (1975) 167–176.
[31] I.F. Gaunt, P. Grasso, I.S. Kiss, S.D. Gangolli, Short-term toxicity study on indigo carmine in the pig, Food Cosmet. Toxicol. 7 (1969) 17–24.
[32] L.E. Fraga, M.A. Anderson, M.L.P.M.A. Beatriz, F.M.M. Paschoal, L.P. Romão, M.V.B. Zanoni, Evaluation of the photoelectrocatalytic method for oxidizing chloride and simultaneous removal of microcystin toxins in surface water, Electrochim. Acta 54 (2009) 2069–2076.
[33] F.M.M. Paschoal, M.A. Anderson, M.V.B. Zanoni, Simultaneous removal of chromium and leather dye from simulated tannery effluent by photoelectrochemistry, J. Hazard. Mater. 166 (2009) 531–537.
[34] H.P. Klug, X-ray Diffraction Procedures for Polycrystalline and Amorphous Materials, 2nd ed., John Wiley & Sons, New York, 1974.

[35] K. Kalyanansundaram, M. Gratzel, Applications of functionalized transition metal complexes in photonic and optoelectronic devices, Coord. Chem. Rev. 77 (1998) 347–414.
[36] M.A. Butler, Photoelectrolysis and physical properties of the semiconducting electrode WO_3, J. Appl. Phys. 48 (1977) 1914–1920.
[37] M.A. Fox, R.B. Draper, M. Dulay, K. OïShea, Photochemical Conversion and Storage of Solar Energy, Kluwer Academic Publications, The Netherlands, 1991.
[38] D. Rajkumar, J.G. Kim, K. Palanivelu, Indirect electrochemical oxidation of phenol in the presence of chloride for wastewater treatment, Chem. Eng. Technol. 28 (2005) 98–105.